

# Elastic Properties of Fullerites and Diamond-Like Phases

Leysan Kh. Rysaeva, Julia A. Baimova,\* Dmitry S. Lisovenko, Valentin A. Gorodtsov, and Sergey V. Dmitriev

Diamond-like structures, that include  $sp^2$  and  $sp^3$  hybridized carbon atoms, are of considerable interest nowadays. In the present work, various carbon auxetic structures are studied by the combination of molecular dynamics (MD) and analytical approach. Two fullerites based on the fullerene  $C_{60}$  and fullerene-like molecule  $C_{48}$  are investigated as well as diamond-like structures based on other fullerene-like molecules (called fulleranes), carbon nanotubes (called tubulanes) and graphene sheets. MD is used to find the equilibrium states of the structures and calculate compliance and stiffness coefficients for stable configurations. Analytical methods are used to calculate the engineering elastic coefficients (Young's modulus, Poisson's ratio, shear modulus and bulk modulus), and to study their transformation under rotation of the coordinate system. All the considered structures are partial auxetics with the negative value of Poisson's ratio for properly chosen tensile directions. It is shown that some of these structures, in a particular tension direction, have a very high Young's modulus, that is, 1852 GPa for tubulane TA6.

## 1. Introduction

The hardest material currently known is diamond, but for many years extensive efforts have been devoted to finding new materials with the hardness exceeding that of diamond. Various cubic phases, for example, lonsdaleite,  $C_{20}$ -T,  $C_3N_4$ ,  $BC_{12}$ , and diamond-like phases (DLP) have been predicted to have outstanding physical and mechanical properties.<sup>[1–12]</sup> Diamond-like structures have  $sp^3$ -hybridized carbon atoms or they can include a small portion of  $sp^2$ -hybridized atoms. Such

structures can be produced by various methods, for example, cold compression,<sup>[13]</sup> shock compression of polycrystalline graphite,<sup>[14,15]</sup> heating of carbon soot,<sup>[16]</sup> transformation of onion structures under high pressure<sup>[17]</sup> to name a few. Superhard materials are of particular importance in industrial applications, such as cutting, polishing, and drilling tools, and surface-protecting coatings.<sup>[18]</sup> It has been already shown that some diamond-like structures have Vickers hardness close to diamond ( $96 \pm 5$  GPa)<sup>[19]</sup>: 93.2 GPa for lonsdaleite, 88.8 GPa for  $BC_8$ ,<sup>[20]</sup>  $\approx 90$  GPa for DLP LA1, LA2,<sup>[3]</sup> etc. Complete information on the structures with the highest values of Vickers hardness and other important characteristics can be found in <http://sacada.sctms.ru>. Results, obtained in the field to date, broaden our understanding of the mechanical properties of diamond-like structures including their

auxeticity<sup>[7,8]</sup> and deformation behavior.<sup>[9]</sup> Several DLPs have been found experimentally and many others have been studied with the help of atomistic modeling methods such as ab-initio simulations or molecular dynamics (MD).


The other class of bulk carbon nanomaterials is based on  $sp^2$  carbon polymorphs bonded by weak van-der-Waals interactions, which can form an immense variety of structures.<sup>[21–32]</sup> Among such nanomaterials, fullerite (a material consisting of fullerene molecules) is well known. The most studied structures are the fullerites based on  $C_{60}$  or  $C_{70}$  fullerenes. They have been produced experimentally<sup>[33,34]</sup> and they can be transformed to the superdense and superhard phases.<sup>[35–37]</sup> At room temperatures,  $C_{60}$  molecules are arranged in a face-centered-cubic (fcc) lattice, while at 259 K a fcc to simple cubic (sc) transition occurs.<sup>[38,39]</sup> It should also be noted that  $C_{60}$  molecules undergo phase transition to polycrystalline diamond at the pressure higher than 20 GPa.<sup>[40]</sup> Despite the fact that fullerite is known for a long time, its mechanical properties and characteristics remain poorly understood. To date, there are studies of the elastic properties of polycrystalline fullerite samples,<sup>[7]</sup> measurements of Young's modulus on single-crystal samples of small dimensions,<sup>[41,42]</sup> and studies of polycrystalline films. Earlier measurements of the elastic constants of some diamond-like structures and fullerite were also performed.<sup>[43–46]</sup> In ref. <sup>[43–46]</sup> quite large (up to 30 mg), well-faceted solid fcc  $C_{60}$  single-crystal with lattice parameter 14.17 Å, fabricated by a growth from the gas phase, is considered. The following elastic moduli of  $C_{60}$  single-crystal were determined from measurements of ultrasound velocities:  $c_{11} \approx 15$  GPa,  $c_{11}$

L. Kh. Rysaeva, Dr. J. A. Baimova, Dr. S. V. Dmitriev  
Institute for Metals Superplasticity Problems of the Russian Academy of Sciences  
Khalturina st. 39, Ufa 450001, Russia  
E-mail: a.baimova@gmail.com

Dr. D. S. Lisovenko, Prof. V. A. Gorodtsov  
Ishlinsky Institute for Problems in Mechanics of the Russian Academy of Sciences  
Vernadsky pr. 101-1, Moscow 119526, Russia

Dr. S. V. Dmitriev  
National Research Tomsk State University  
Lenin Ave 36, Tomsk 634050, Russia

Dr. Julia A. Baimova  
Bashkir State University  
Zaki Validi St. 32, Ufa 450076, Russia

 The ORCID identification number(s) for the author(s) of this article can be found under <https://doi.org/10.1002/pssb.201800049>.

DOI: 10.1002/pssb.201800049

$\approx 9$  GPa, and  $c_{44} \approx 6$  GPa,<sup>[43]</sup> the effect of relaxation,<sup>[44]</sup> and the temperature<sup>[45,46]</sup> on the elastic moduli were also investigated.

It has been shown that carbon nanostructures such as single-wall nanotubes,<sup>[47,48]</sup> carbon nanotube sheets,<sup>[49]</sup> and graphene<sup>[50,51]</sup> can have negative Poisson's ratio. In ref. <sup>[51]</sup> auxetic properties were found for graphene with 5-8-5 defects. It was also shown that minimal Poisson's ratio for such structures is equal to  $-0.3$ . In ref. <sup>[52]</sup> negative Poisson's ratio was found for hydrostatically stretched graphene in the range of strain  $\epsilon_{xx} = \epsilon_{yy} > 0.12$ . In ref. <sup>[53]</sup> the effect of hydrostatic pressure on the elastic properties of hexagonal crystals was studied. It was shown that for graphite negative Poisson's ratio can be found under negative pressure.

Structures considered in the present work belong to different crystal systems. For many anisotropic materials of various crystal systems (cubic,<sup>[54-72]</sup> hexagonal,<sup>[61,62,73-76]</sup> rhombohedral<sup>[61,62,77-79]</sup>, tetragonal<sup>[61,62,80-82]</sup>, orthorhombic<sup>[61,62,78,83-85]</sup>, monoclinic,<sup>[61,62,74,86,87]</sup> and triclinic<sup>[87]</sup>) negative Poisson's ratio was observed. To date, more than 450 crystals with negative Poisson's ratio (auxetic crystals) were found. More than 300 were found among the crystals with cubic anisotropy.<sup>[65,67]</sup> Studies of auxetic structures have been conducted for many decades and some of the

results are debated till now. For example, in ref. <sup>[88]</sup> it was shown that Cd has negative Poisson's ratio, which was proved to be wrong.<sup>[89]</sup> This mistake is connected with the wrong calculation of the compliance coefficients and it was shown that Poisson's ratio of Cd ranges from 0.1 to 0.7.<sup>[89,90]</sup>

In this study, the results on the investigation of structure and auxetic properties of carbon nanostructures with  $sp^3$  (DLPs) and  $sp^2$  (fullerites) hybridization are presented. The results obtained by the MD simulations are used to calculate the engineering elasticity constants from analytical equations. For auxetic structures of various anisotropy, compliance and stiffness constants, Poisson's ratio, bulk modulus, shear modulus, and Young's modulus are presented.

## 2. Simulation Details

Building units of the carbon structures studied here are shown in the first row of **Figure 1**. Fullerites of  $C_{60}$  or  $C_{48}$  fullerenes packed in fcc or sc lattices are considered. Diamond-like phases called fulleranes are based on fullerene-like molecules  $C_6$ ,  $C_8$ , and  $C_{48}$ .

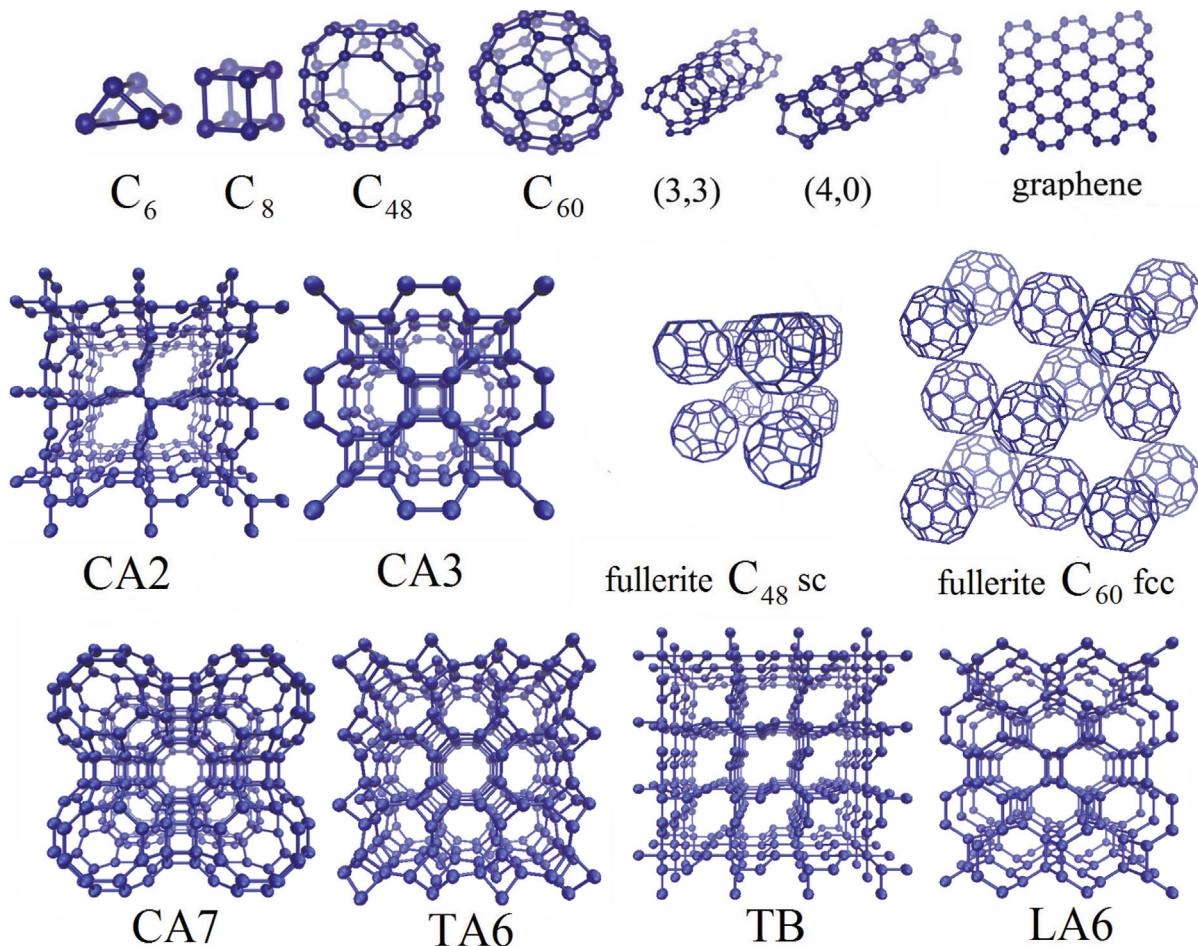


**Figure 1.** First row gives building elements of the structures considered in this study. Second and third rows give the studied three-dimensional structures. Among them are two fullerites with cubic anisotropy: fcc packing of  $C_{60}$  and sc packing of  $C_{48}$ . The CA2 fullerane has hexagonal anisotropy. CA3 and CA7 fulleranes have cubic anisotropy. LA6 DLP based on graphene sheet is of orthorhombic anisotropy. TB and TA6 tubulanes are of hexagonal and tetragonal anisotropy, respectively.

DLP called tubulanes are based on (4,0) or (3,3) carbon nanotubes. LA<sub>6</sub> DLP defined in ref. [3–6] is composed of graphene sheets.

Initial structures were generated using a home-made program, which allows to combine different structural elements into three-dimensional structures. Initial structures studied here are presented in the second and third rows of Figure 1 and they possess cubic, tetragonal, hexagonal, or orthorhombic anisotropy. Among them are two fullerites with cubic anisotropy composed of C<sub>60</sub> and C<sub>48</sub>, packed in fcc and sc lattices, respectively. The CA2 fullerane has hexagonal anisotropy. CA3 and CA7 fulleranes have cubic anisotropy. LA6 DLP based on graphene sheets is of orthorhombic anisotropy. TB and TA6 tubulanes are of hexagonal and tetragonal anisotropy, respectively.

Structure relaxation and calculations of the compliance coefficients are carried out using the LAMMPS package<sup>[91]</sup> with the AIREBO interatomic potential,<sup>[92]</sup> which was successfully used to study the mechanical and thermal properties of various carbon systems. It should be noted, that AIREBO potential has some limitations, for example, cannot be used for simulation of amorphous or melted carbon structures,<sup>[93,9]</sup> nucleation of carbon nanostructures or their damage,<sup>[94,95]</sup> investigation of hybrid sp<sup>2</sup>-sp<sup>3</sup> carbon nanostructures.<sup>[96]</sup> Despite in real life DLP can have mixed sp<sup>2</sup>-sp<sup>3</sup>-hybridization, in the present work application of periodic boundary conditions lead to the consideration of only sp<sup>3</sup> DLP structures. The methodology proposed in the present work was previously successfully applied for the investigation of the aucticity of various DLP.<sup>[7,8,52]</sup> All the structures are firstly relaxed until a local or global minimum of potential energy is reached. After that, all the structural parameters are calculated. All the calculations are conducted at 1 K so that the effect of temperature on the elastic constants was not analyzed.

Stiffness coefficients for all the considered structures are calculated from MD calculations. The following scheme is used: single-component stress is applied to the structure and the corresponding strain components are calculated. The applied stress is chosen in such a way that the resulting strains do not exceed 1%, in order to remain in the Hooke's law regime.

Stiffness coefficients for orthorhombic anisotropy are calculated from the Hooke's law as follows:

- 1) uniaxial tensile stress  $\sigma_{xx}$  is applied, the resulting nonzero strains  $\varepsilon_{xx}$  and  $\varepsilon_{yy}$  are determined to find

$$s_{11} = \frac{\varepsilon_{xx}}{\sigma_{xx}}, \quad s_{12} = \frac{\varepsilon_{yy}}{\sigma_{xx}}$$

- 2) uniaxial tensile stress  $\sigma_{zz}$  is applied, nonzero strains  $\varepsilon_{zz}$ ,  $\varepsilon_{xx}$ , and  $\varepsilon_{yy}$  are determined to find

$$s_{13} = \frac{\varepsilon_{xx}}{\sigma_{zz}}, \quad s_{23} = \frac{\varepsilon_{yy}}{\sigma_{zz}}, \quad s_{33} = \frac{\varepsilon_{zz}}{\sigma_{zz}}$$

- 3) tensile stress  $\sigma_{yy}$  is applied, nonzero strains  $\varepsilon_{yy}$  is determined to find

$$s_{22} = \frac{\varepsilon_{yy}}{\sigma_{yy}}$$

- 4) shear stress  $\sigma_{yz}$  is applied and  $\varepsilon_{yz}$  is determined to find  
 $\sigma_{yz}$  is applied and  $\varepsilon_{yz}$  is determined to find

$$s_{44} = \frac{\varepsilon_{yz}}{\sigma_{yz}}$$

- 5) shear stress  $\sigma_{xz}$  is applied and  $\varepsilon_{xz}$  is determined to calculate

$$s_{55} = \frac{\varepsilon_{xz}}{\sigma_{xz}}$$

- 6) shear stress  $\sigma_{xy}$  is applied and  $\varepsilon_{xy}$  is determined to calculate

$$s_{66} = \frac{\varepsilon_{xy}}{\sigma_{xy}}$$

For the calculations of the compliance coefficients for orthorhombic anisotropy the following equations are used:

$$c_{11} = \frac{s_{22}s_{33} - s_{23}^2}{s}, \quad c_{12} = \frac{s_{13}s_{23} - s_{12}s_{33}}{s}$$

$$c_{13} = \frac{s_{12}s_{23} - s_{23}s_{11}}{s}, \quad c_{22} = \frac{s_{11}s_{33} - s_{13}^2}{s}$$

$$c_{23} = \frac{s_{12}s_{13} - s_{23}s_{11}}{s}, \quad c_{33} = \frac{s_{11}s_{22} - s_{12}^2}{s}$$

$$c_{44} = \frac{1}{s_{44}}, \quad c_{55} = \frac{1}{s_{55}}, \quad c_{66} = \frac{1}{s_{66}}$$

where

$$s = (s_{11}s_{22} - s_{12}^2)s_{33} + 2s_{12}s_{13}s_{23} - s_{11}s_{23}^2 - s_{22}s_{13}^2$$

All these equations can be used for the calculation of the compliance coefficients of the phases with higher symmetry under the following simplifications:  $s_{11} = s_{22}$ ,  $s_{44} = s_{55}$ ,  $s_{13} = s_{23}$  for tetragonal anisotropy,  $s_{11} = s_{22}$ ,  $s_{44} = s_{55}$ ,  $s_{13} = s_{23}$ ,  $s_{66} = 2(s_{11} - s_{12})$  for hexagonal anisotropy, and  $s_{11} = s_{22} = s_{33}$ ,  $s_{44} = s_{55} = s_{66}$ ,  $s_{12} = s_{13} = s_{23}$  for cubic anisotropy.

## 3. Results and Discussion

### 3.1. Elastic Properties

The compliance coefficients for all studied structures, obtained by the MD method, are presented in Table 1.

Based on the compliance coefficients presented in Table 1, the variability of Young's modulus, Poisson's ratio and shear modulus is analyzed. Young's modulus for anisotropic structures depends on the tensile direction with respect to crystallographic axis. Poisson's ratio also depends on the direction of measuring the lateral strain. In the linear elasticity theory, Young's modulus  $E(\mathbf{n})$  and Poisson's ratio  $\nu(\mathbf{n}, \mathbf{m})$  depend on the tensor compliance coefficients  $s_{ijkl}$ , unit vector  $\mathbf{n}$  oriented along the tensile direction, and unit vector  $\mathbf{m}$  normal to the tensile direction,<sup>[97]</sup>

$$E^{-1}(\mathbf{n}) = s_{ijkl}n_i n_j n_k n_l \quad (1)$$

**Table 1.** Compliance coefficients  $s_{ij}$  and stiffness coefficients  $c_{ij}$  of carbon nanostructures (fullerites, fullerenes, tubulanes, and DLP based on graphene sheet):  $C_{48}$  sc,  $C_{60}$  fcc, CA3 and CA7 with cubic anisotropy; CA2 and TB with hexagonal anisotropy; TA6 with tetragonal anisotropy; LA6 with orthorhombic anisotropy.

Structure	$s_{11}$ [GPa <sup>-1</sup> ]	$s_{22}$ [GPa <sup>-1</sup> ]	$s_{33}$ [GPa <sup>-1</sup> ]	$s_{44}$ [GPa <sup>-1</sup> ]	$s_{55}$ [GPa <sup>-1</sup> ]	$s_{66}$ [GPa <sup>-1</sup> ]	$s_{12}$ [GPa <sup>-1</sup> ]	$s_{13}$ [GPa <sup>-1</sup> ]	$s_{23}$ [GPa <sup>-1</sup> ]
Fullerites									
$C_{48}$ sc	10.5			6.61			-4.68		
$C_{60}$ fcc	0.052			0.035			-0.0224		
Structure	$s_{11}$ [TPa <sup>-1</sup> ]	$s_{22}$ [TPa <sup>-1</sup> ]	$s_{33}$ [TPa <sup>-1</sup> ]	$s_{44}$ [TPa <sup>-1</sup> ]	$s_{55}$ [TPa <sup>-1</sup> ]	$s_{66}$ [TPa <sup>-1</sup> ]	$s_{12}$ [TPa <sup>-1</sup> ]	$s_{13}$ [TPa <sup>-1</sup> ]	$s_{23}$ [TPa <sup>-1</sup> ]
Fullerenes									
CA2	2.515		1.92	18.4			0.0906	-0.3625	
CA3	1.87			2.496			-0.44		
CA7	8.125			3.64			-3.82		
Tubulanes									
TA6	1.471		0.8194	4.727		2.773	-0.0094	-0.126	
TB	1.656		0.999	10.174			-0.1597	-0.29	
DLP based on graphene sheet									
LA6	2.458	2.238	1.21	2.159	2.363	2.527	-1.408	-0.354	-0.138
Structure	$c_{11}$ [MPa]	$c_{22}$ [MPa]	$c_{33}$ [MPa]	$c_{44}$ [MPa]	$c_{55}$ [MPa]	$c_{66}$ [MPa]	$c_{12}$ [MPa]	$c_{13}$ [MPa]	$c_{23}$ [MPa]
Fullerites									
$C_{48}$ sc	331			151			265		
Fullerenes									
$C_{60}$ fcc	55.3			28.7			41.8		
Fullerenes									
CA2	413		555	161			-1.63	87.3	
CA3	625			400			192		
CA7	750			275			667		
Tubulanes									
TA6	1854		1214	442		221	55.0	-8.59	
TB	600		1067	3614			-30.5	155	
DLP based on graphene sheet									
LA6	709	751	928	418	395	505	462	260	221

$$\nu(\mathbf{n}, \mathbf{m}) = -\frac{s_{ijkl}m_i m_j n_k n_l}{s_{\alpha\beta\lambda\mu}n_\alpha n_\beta n_\lambda n_\mu} \quad (2)$$

Shear modulus  $G(\mathbf{n}, \mathbf{m})$  is defined by vector  $\mathbf{n}$  which is unit vector normal to the slip plane and unit vector  $\mathbf{m}$  showing the slip direction<sup>[97]</sup>

$$G^{-1}(\mathbf{n}, \mathbf{m}) = 4s_{ijkl}n_i m_j n_k m_l. \quad (3)$$

The variability of Young's modulus, Poisson's ratio and shear modulus are defined by Euler's angles  $\varphi$ ,  $\theta$ , and  $\psi$  instead of unit

vectors. Unit vectors  $n$  and  $m$  are related to the Euler's angles as follows

$$\mathbf{n} = \begin{pmatrix} \sin \varphi \sin \theta \\ -\cos \varphi \sin \theta \\ \cos \theta \end{pmatrix} \quad (4)$$

$$\mathbf{m} = \begin{pmatrix} -\sin \varphi \cos \theta \cos \psi - \cos \varphi \sin \psi \\ \cos \varphi \cos \theta \cos \psi - \sin \varphi \sin \psi \\ \sin \theta \cos \psi \end{pmatrix} \quad (5)$$

### 3.1.1. Carbon Nanostructures with Cubic Anisotropy

Equations for the calculation of Young's modulus and Poisson's ratio can be written as follows [65,98]

$$\frac{1}{s_{11}E} = 1 - \frac{\delta}{2}M(\varphi, \theta) \quad (6)$$

$$\frac{\nu}{s_{11}E} = -\frac{\delta}{2}[N(\varphi, \theta, \psi) - \Pi] \quad (7)$$

$$\frac{1}{s_{44}G} = 1 + (A - 1)N(\varphi, \theta, \psi) \quad (8)$$

$$\Pi \equiv -\frac{2s_{12}}{\Delta}, \quad \delta \equiv \frac{\Delta}{s_{11}}$$

$$A \equiv 2\frac{s_{11} - s_{12}}{s_{44}} = 2\frac{c_{44}}{c_{11} - c_{12}}$$

$$0 \leq M \equiv \sin^2 2\theta + \sin^4 \theta \sin^2 2\varphi \leq \frac{4}{3}$$

$$0 \leq N \equiv 3 \sin^2 \theta \cos^2 \theta \cos^2 \psi + (\cos \theta \cos 2\varphi \cos \psi - \sin \psi)^2 \sin^2 \theta \leq 1$$

Here  $\Delta \equiv s_{11} - s_{12} - 0.5s_{44}$  is the anisotropy parameter for the cubic crystals,  $A$  is the Zener anisotropy parameter.

For cubic anisotropy, Young's modulus has three extremal values<sup>[99]</sup> corresponding to the tensile directions [100], [110], and [111]:

$$E_{[100]} = \frac{1}{s_{11}} \quad (9)$$

$$E_{[110]} = \frac{1}{s_{11} - \Delta/2} \quad (10)$$

$$E_{[111]} = \frac{1}{s_{11} - 2\Delta/3} \quad (11)$$

**Table 2.** Extreme values of Young's modulus, anisotropy parameter  $\Delta$ , and  $\alpha = E_{\max}/E_{\min}$  of fullerites and fullerenes with cubic anisotropy.

Structure	$\Delta$ [GPa <sup>-1</sup> ]	$E_{[100]}$ [MPa]	$E_{[110]}$ [MPa]	$E_{[111]}$ [MPa]	$\alpha$
Fullirites					
C <sub>48</sub> sc	11.9	95.1	219	<b>386</b>	4.06
Fullerenes					
CA3	1.06	535	746	<b>860</b>	1.61
CA7	10.1	123	327	<b>728</b>	5.92

Bold values signify the maximum values of Young's modulus.

For cubic crystals with positive anisotropy parameter,  $\Delta > 0$ , from (9)–(11) it follows  $E_{[111]} > E_{[110]} > E_{[100]}$ . For cubic crystals with negative anisotropy parameter,  $\Delta < 0$ , the opposite inequalities take place  $E_{[100]} > E_{[110]} > E_{[111]}$ . In **Table 2**, the extreme values of Young's modulus and values of the anisotropy parameter  $\Delta$  are given. They are determined from the values of the elastic constants of equilibrium structures presented in Table 1. Bold font in Table 2 emphasizes the maximum values of Young's modulus. For all the considered structures maximal Young's moduli are observed for tension along [111] direction since all of the considered structures have positive anisotropy parameter (see Table 2). Highest Young's modulus for the structures with cubic anisotropy is found for CA7 (728 GPa). The highest difference between maximal and minimal values of Young's modulus is also found for CA7 ( $E_{\max}/E_{\min} = 5.92$ ).

In **Table 3**, dimensionless parameters  $\Pi$  and  $\delta$ , maximal  $\nu_{\min}$  and minimal  $\nu_{\max}$  Poisson's ratios as well as Poisson's ratios for particular crystallographic orientations are presented. Analysis of the variability of Poisson's ratio showed that four nanostructures with the cubic anisotropy have negative Poisson's ratio (see Table 3). All of the considered structures are partial auxetics ( $0 < \Pi < 1$ ) in accordance with the classification proposed in ref. [65]. Lowest Poisson's ratio is found for CA7 ( $\nu_{\min} = -0.40$ ) as well as the highest difference between maximal and minimal Poisson's ratios ( $\nu_{\max} - \nu_{\min} = 1.65$ ). For fullerite C<sub>60</sub> minimal Poisson's ratio is equal to  $-0.26$  and for fullerite C<sub>48</sub> it is equal to  $-0.28$ . Averaged Poisson's ratio for all

**Table 3.** Extremal values of Poisson's ratio (global maxima and minima  $\nu_{\max}$ ,  $\nu_{\min}$ , for particular orientations  $\nu_{[100],[001]}$ ,  $\nu_{[001],[110]}$ ,  $\nu_{[110],[110]}$ , and  $\nu_{(111),(111)}$ ) and dimensionless parameters  $\Pi$  and  $\delta$  for fullerites and fullerenes.

Structure	$\Pi$	$\delta$	$\nu_{\min}$	$\nu_{\max}$	$\nu_{[100],[001]}$	$\nu_{[001],[110]}$	$\nu_{[110],[110]}$	$\nu_{(111),(111)}$
Fullirites								
C <sub>48</sub> sc	0.787	1.13	-0.28	1.02	0.44	1.02	-0.28	0.28
C <sub>60</sub> fcc	0.788	1.10	-0.26	0.96	0.43	0.95	-0.26	0.24
Fullerenes								
CA3	0.830	0.57	-0.07	0.33	0.24	0.33	-0.07	0.07
CA7	0.755	1.25	-0.40	1.25	0.47	1.25	-0.41	0.33



the structures is positive. In **Figure 2** the auxeticity surface ( $\nu = 0$ ) for fcc fullerite  $C_{60}$  is constructed in the space of Euler's angles with the periods  $T_\varphi = \pi/2$ ,  $T_\theta = 2\pi$ , and  $T_\psi = \pi$ . The auxeticity zone ( $\nu < 0$ ) is inside the presented surface. From these surfaces, one can determine Euler's angles, that is, the directions of stretching for which negative Poisson's ratio is observed. The auxeticity surface of sc fullerite  $C_{48}$  is very similar to that of  $C_{60}$  because they have nearly same parameters  $\Pi$  and  $\delta$ . Auxeticity surfaces for CA3 and CA7 were previously presented in ref. [8]. As it can be seen from Table 3, the biggest auxeticity zone is observed for CA7, since it has the lowest values of the dimensionless parameters  $\Pi$  and  $\delta$ .

Poisson's ratio for particular orientations are defined as follows

$$\nu_{[100],[001]} = \frac{\Pi\delta}{2}$$

$$\nu_{[001],[110]} = \frac{\Pi\delta}{2 - \delta}$$

$$\nu_{[1\bar{1}0],[110]} = \frac{\delta(\Pi - 1)}{2 - \delta}$$

$$\nu_{[111],[111]} = \frac{\delta(1.5\Pi - 1)}{3 - 2\delta}$$

The last three indices indicate the directions of stretching, and the first three indices indicate the direction of the lateral strain measurement. The analysis of these equations with the use of thermodynamic limitations of the positivity of the determination of elastic energy  $\Pi\delta > 2\delta - 2$ ,  $1 > \Pi\delta > -2$ , and  $\delta < 1.5$ [65] shows:

1)  $\Pi > 0$ ,  $0 < \delta < 1.5$ :

$$\nu_{[001],[110]} > \nu_{[100],[001]} > \nu_{(111),[111]} > \nu_{[1\bar{1}0],[110]}$$

2)  $\Pi > 0$ ,  $\delta < 0$ :

$$\nu_{[1\bar{1}0],[110]} > \nu_{(111),[111]} > \nu_{[001],[110]} > \nu_{[100],[001]}$$

3)  $\Pi < 0$ ,  $\delta < 0$ :

$$\nu_{[1\bar{1}0],[110]} > \nu_{(111),[111]} > \nu_{[100],[001]} > \nu_{[001],[110]}$$

4)  $\Pi < 0$ ,  $0 < \delta < 1.5$ :

$$\nu_{[100],[001]} > \nu_{[001],[110]} > \nu_{(111),[111]} > \nu_{[1\bar{1}0],[110]}$$

All the considered structures with cubic anisotropy have  $\Pi > 0$  and  $0 < \delta < 1.5$ , which means that the values of the Poisson's ratio for particular orientations satisfy the above conditions.

The analysis of formula (8) for the shear modulus makes it possible to determine the maximum and minimum values[98]:

$$G_1 = \frac{1}{s_{44}} \quad (12)$$

$$G_2 = \frac{1}{2(s_{11} - s_{12})} \quad (13)$$

Zener anisotropy parameter will affect the extremal values of the shear modulus ( $G_1$  and  $G_2$ ) and will define which one became minima or maxima. For the cubic crystals with  $A > 1$  (or positive anisotropy  $\Delta > 0$ ) from (12) and (13) it is seen that  $G_1 > G_2$ . For crystals with  $0 < A < 1$  (or negative anisotropy  $\Delta < 0$ ) the reverse inequality takes place  $G_1 < G_2$ . For all the considered cubic structures the value of Zener anisotropy parameter is greater than 1 (see **Table 4**), which means that  $G_1$  is the maximal value. Zener anisotropy parameters, extremal values of the shear modulus, and values of bulk modulus are presented in Table 4. The values of the bulk modulus are calculated as  $B = (c_{11} + 2c_{12})/3$ . The greatest shear anisotropy is found for CA7 ( $G_{\max}/G_{\min} = 6.56$ ). The

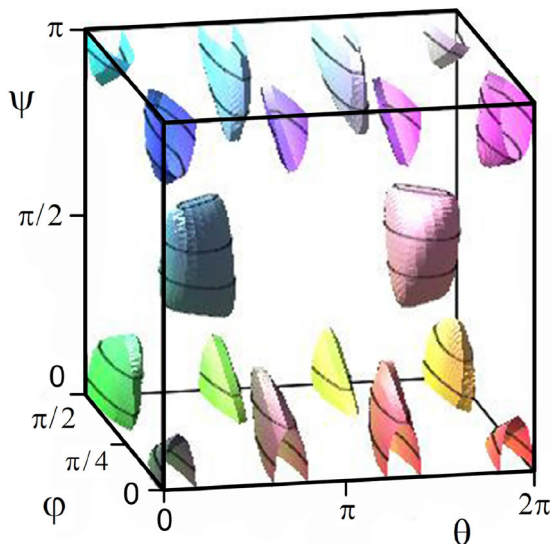


**Figure 2.** Auxeticity surfaces ( $\nu = 0$ ) of fullerite  $C_{60}$  with cubic anisotropy.

**Table 4.** Extremal values of shear modulus, Zener's anisotropy parameter  $A$ ,  $\beta = G_{\max}/G_{\min}$ , and bulk modulus  $B$  of fullerites and fullerenes with cubic anisotropy.

Structure	$A$	$G_1$ [MPa]	$G_2$ [MPa]	$\beta$	$B$ [MPa]
Fullerites					
$C_{48}$ sc	4.60	<b>151</b>	32.9	4.59	287
Structure	$A$	$G_1$ [GPa]	$G_2$ [GPa]	$\beta$	$B$ [GPa]
Fullerites					
$C_{60}$ fcc	4.28	<b>28.7</b>	6.72	4.27	46.3
Fullerenes					
CA3	1.85	<b>400</b>	216	1.85	337
CA7	6.56	<b>275</b>	41.9	6.56	694

Bold values signify the maximum values of Young's modulus.

highest shear modulus is found for CA3 (400 GPa) and the lowest is for C<sub>48</sub> ( $G_{1\min} = 32.9$  MPa). The highest bulk modulus is observed for CA7 (694 GPa) and the lowest is for the fullerite C<sub>48</sub> (287 MPa).

### 3.1.2. Carbon Nanostructures with Hexagonal Anisotropy

For the structures with hexagonal anisotropy Young's modulus and Poisson's ratio are defined as<sup>[75,89]</sup>:

$$\frac{1}{s_{11}E} = 1 + (\Pi_1 - \Pi_{01} \sin^2 \theta) \cos^2 \theta \quad (14)$$

$$-\frac{\nu}{s_{13}E} = 1 + (\Pi_2 \sin^2 \psi + \Pi_{02} \cos^2 \theta \cos^2 \psi) \sin^2 \theta \quad (15)$$

$$\frac{1}{s_{44}G} = 1 + (\Pi_3 \sin^2 \psi + 4\Pi_{03} \cos^2 \theta \cos^2 \psi) \sin^2 \theta \quad (16)$$

$$\Pi_{01} \equiv \frac{\delta}{s_{11}}, \quad \Pi_{02} \equiv \frac{\delta}{s_{13}}, \quad \Pi_{03} \equiv \frac{\delta}{s_{44}}$$

$$\Pi_1 \equiv \frac{s_{33} - s_{11}}{2s_{11} - 2s_{12} - s_{44}}, \quad \Pi_2 \equiv \frac{s_{12} - s_{13}}{s_{13}}$$

$$\Pi_3 \equiv \frac{s_{11} - 2s_{12} - s_{44}}{s_{44}}$$

$$\delta \equiv s_{11} + s_{33} - 2s_{13} - s_{44}$$

The analysis of Young's modulus presented in ref. [75] showed that three extreme values can be calculated:

$$E_1 = E_{[0001]} = \frac{1}{s_{33}}$$

$$E_2 = E_{[2\bar{1}10]} = \frac{1}{s_{11}}$$

and

$$E_3 = \frac{4\Pi_{01}}{4\Pi_{01} - (\Pi_1 - \Pi_{01})^2 s_{11}} \frac{1}{s_{11}} > 0$$

at

$$\cos^2 \theta = \frac{\Pi_{01} - \Pi}{2\Pi_{01}}$$

Structures CA2 and TB have hexagonal anisotropy and three extremal values for Young's modulus for these structures are presented in Table 5, while Young's modulus are illustrated as the function of  $\theta$  in Figure 3. The highest value among hexagonal structures is found for tubulane TB ( $E_{\max} = 1730$  GPa at  $\theta = 38.1^\circ$ ), which is three times higher than maximal Young's modulus for

**Table 5.** Extremal values of Young's modulus  $E$ , shear modulus  $G$ , and bulk modulus  $B$  for CA2 fullerene and TB tubulane.

Structure	$E_1$ [GPa]	$E_2$ [GPa]	$E_3$ [GPa]	$B$ [GPa]
Fullerene				
CA2	<b>518</b>	398	393	192
Tubulane				
TB	983	573	<b>1730</b>	314
Structure	$G_1$ [GPa]	$G_2$ [GPa]	$G_3$ [GPa]	$G_4$ [GPa]
Fullerene				
CA2	54.3	<b>206</b>	194	120
Tubulane				
TB	98.3	275	<b>309</b>	193

Bold values signify the maximum values of Young's modulus.

fullerene CA2 ( $E_{1\max} = E_{[0001]} = 518$  GPa). The minimal value of Young's modulus for TB ( $E_{\min} = 573$  GPa) is found at tension along  $[2\bar{1}10]$ . Bulk modulus  $B$  for hexagonal structures is also presented in Table 5. To calculate bulk modulus the following equation is used  $B = (2c_{11} + c_{33} + 2c_{12} + 4c_{13})/9$ . Bulk modulus of tubulane TB is 1.6 times higher than for fullerene CA2.

The analysis of variability of shear modulus presented in ref. [89] showed that for hexagonal structures four stationary values can be found:

$$G_1 = \frac{1}{s_{44}}$$

for  $\theta = 0$  and any  $\psi$  angles, and also at  $\theta = \pi/2$ ,  $\psi = 0$ ;

$$G_2 = \frac{1}{s_{44}(1 + \Pi_3)} = \frac{1}{s_{66}}$$

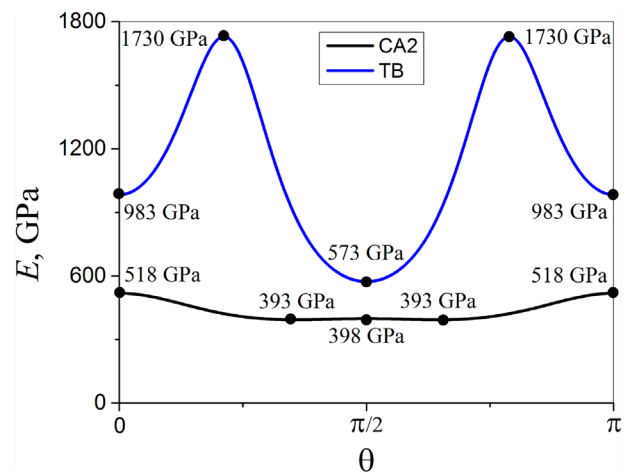


**Figure 3.** Variability of Young's modulus of diamond-like structure CA2 (black curve) and tubulane TB (blue curve) with hexagonal anisotropy. Dots mark extreme values of Young's modulus.

is obtained at  $\theta = \psi = \pi/2$ ;

$$G_3 = \frac{1}{s_{44}(1 + \Pi_{03})} = \frac{1}{s_{11} + s_{33} - 2s_{13}}$$

is achieved at  $\theta = \pi/4$ ,  $\psi = 0$ , and  $\theta = 3\pi/4$ ,  $\psi = 0$ ;

$$G_4^{-1} = s_{44} \left( 1 + \Pi_3 - \frac{\Pi_3^2}{4\Pi_{03}} \right)$$

possible for  $\theta_0$ ,  $\psi_0$  at  $0 \leq \cos^2\theta_0 = 0.25\Pi_3/\Pi_{03} \leq 1$ ,  $0 \leq \cos^2\psi_0 = \Pi_3/(4\Pi_{03} - \Pi_3) \leq 1$ . The first three stationary values can be extremal. Extremal values of shear modulus for TB and CA2 are presented in Table 5. The maximal values are  $G_{2 \max} = 206$  GPa for CA2 and  $G_{3 \max} = 309$  GPa for tubulane TB.

Poisson's ratio for hexagonal crystals have eight stationary values.<sup>[53]</sup> The first three values are simply calculated as follows:

$$v_1 = v_{(0001),[0001]} = -\frac{s_{13}}{s_{33}}$$

$$v_2 = v_{[2\bar{1}10],[01\bar{1}0]} = -\frac{s_{13}}{s_{11}}$$

**Table 6.** Stationary values of Poisson's ratio for CA2 fullerene and TB tubulane.

Structure	$v_1$	$v_2$	$v_3$	$v_4$	$v_5$	$v_6$	$v_7$	$v_8$
Fullerene								
CA2	0.21	0.16	<b>-0.04</b>	<b>0.27</b>	-	-	-	-
Tubulane								
TB	0.27	0.16	-0.09	-	<b>-0.80</b>	<b>0.29</b>	-	-0.08

Bold values signify the maximum values of Young's modulus.

$$v_3 = v_{[000\bar{1}],[01\bar{1}0]} = -\frac{s_{12}}{s_{11}}$$

The equations for the other five stationary values are presented in ref.<sup>[53]</sup> Poisson's ratio for CA2 and TB is presented in Table 6. Both structures have negative Poisson's ratio. For tubulane TB, four negative values are observed. The most negative Poisson's ratio among hexagonal structures is found for TB ( $v_{\min} = -0.80$ ). Minimal Poisson's ratio for CA2 is found for tension along  $[01\bar{1}0]$  and equal to  $v_{\min} = v_{[000\bar{1}],[01\bar{1}0]} = -0.04$ . Auxeticity surfaces for CA2 and TB are presented in Figure 4a and b. In Figure 4c and d auxeticity curve ( $v = 0$ ) calculated as

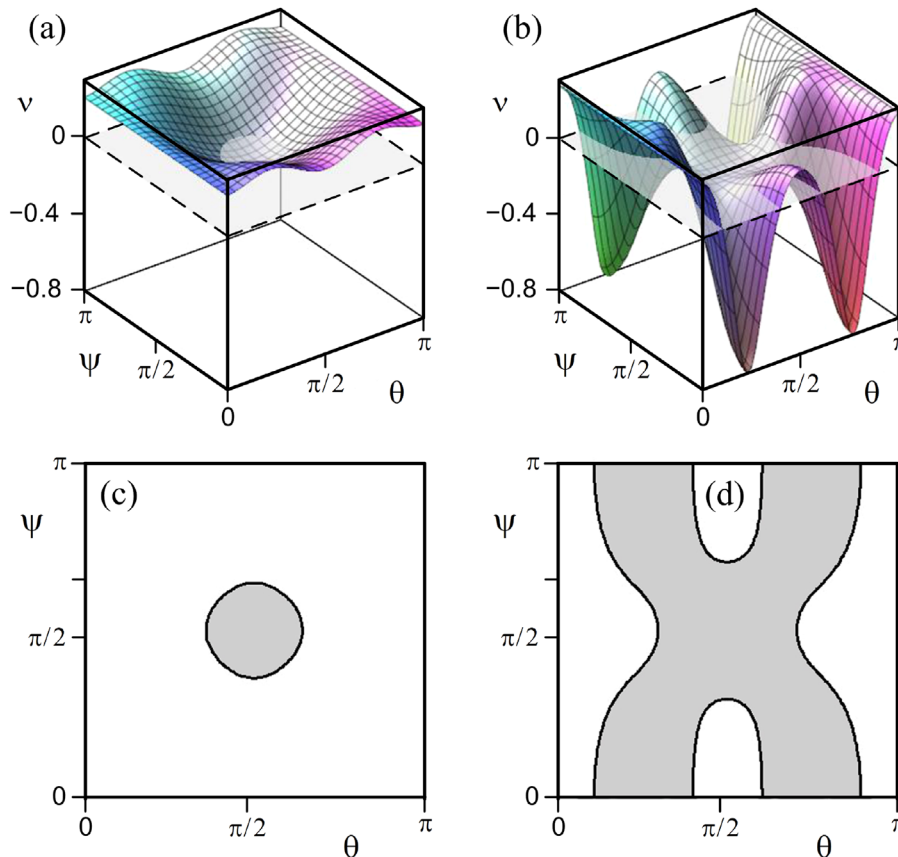


**Figure 4.** The surfaces of Poisson's ratio for diamond-like structure CA2 (a) and tubulane TB (b) and auxeticity curves ( $v = 0$ ) for diamond-like structure CA2 (c) and tubulane TB (d). The auxeticity zone ( $v = 0$ ) is shown in gray.



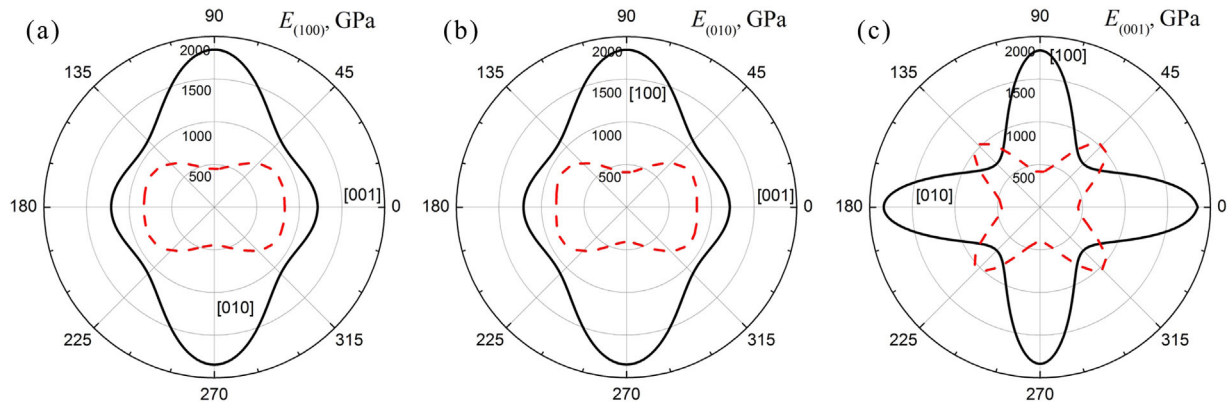


**Figure 5.** Orientational dependences of Young's moduli in the (100) (a), (010) (b), (001) (c) planes for TA6 tubulane (black solid lines) and LA6 DLP based on graphene (red dashed lines).

$$s_{13} + ((s_{12} - s_{13})\sin^2\psi + \delta\cos^2\theta\cos^2\psi)\sin^2\theta = 0$$

is presented. Auxeticity zone is shown by gray. As it can be seen from Figure 4 the bigger auxeticity zone is found for tubulane TB.

### 3.1.3. Carbon Nanostructures with Orthorhombic and Tetragonal Anisotropy

For investigation of these structures, (100), (010), (001) planes are taken. Under tension along these planes and from Equations (1), (3–5), Young's modulus  $E$  as the function of orientation angle (angle between tensile direction and crystallographic axis) can be found as

$$E_{(100)}^{-1}(\theta) = s_{22}\sin^4\theta + s_{33}\cos^4\theta + (2s_{23} + s_{44})\sin^2\theta\cos^2\theta \quad (17)$$

$$E_{(010)}^{-1}(\theta) = s_{11}\sin^4\theta + s_{33}\cos^4\theta + (2s_{13} + s_{55})\sin^2\theta\cos^2\theta \quad (18)$$

$$E_{(001)}^{-1}(\varphi) = s_{11}\sin^4\varphi + s_{22}\cos^4\varphi + (2s_{12} + s_{66})\sin^2\varphi\cos^2\varphi \quad (19)$$

where angle  $\theta$  is calculated in (100) (at  $\varphi = 0$ ), (010) (at  $\varphi = \pi/2$ ) planes from [001] direction and angle  $\varphi$  in (001) plane (at  $\theta = \pi/2$ ) from [010] direction. Shear modulus are calculated in these planes as follows

$$G_{(100)}^{-1} = s_{55}\sin^2\psi + s_{66}\cos^2\psi \quad (20)$$

$$G_{(010)}^{-1} = s_{44}\sin^2\psi + s_{66}\cos^2\psi \quad (21)$$

$$G_{(001)}^{-1} = s_{44}\sin^2\psi + s_{55}\cos^2\psi \quad (22)$$

where angle  $\psi$  is calculated in (100) and (001) planes from [010] direction and in (010) plane from  $[\bar{1}00]$  direction. Equations

(17–22) for (100), (010), (001) planes are used for structures with tetragonal anisotropy at  $s_{11} = s_{22}$ ,  $s_{44} = s_{55}$ ,  $s_{13} = s_{23}$ .

The orientation dependences of Young's modulus for TA6 and LA6 in (100), (010), and (001) planes are presented in **Figure 5**. As it can be seen, Young's modulus for TA6 tubulane is higher than that for LA6 in planes (100) and (010). Maximal values of Young's modulus for TA6 in these planes is equal to 1852 GPa for tension directions [100] and [010] (see also **Table 7**). This value is higher than maximal Young's modulus for graphene (1.02 TPa)<sup>[100]</sup> It should be mentioned that Young's modulus for tubulanes is highest among the carbon nanostructures under consideration. Minimal Young's modulus for TA6 for tension in (100) and (010) planes is equal to 1075 GPa and observed for angles close to 45°. For LA6 structure for tension in (100) plane maximal Young's modulus is  $E_{\max} = 838$  GPa and observed for angle of 21.2°. For (010) plane maximal value of Young's modulus is 861 GPa at  $\theta = 22.9^\circ$ . For tension in (001) plane the significant difference between maximal and minimal Young's modulus for TA6 and LA6 is found ( $E_{\max}/E_{\min} = 2.58$ ,  $E_{\min} = 717$  GPa at  $\varphi = 45^\circ$  for TA6 and  $E_{\max}/E_{\min} = 2.55$ ,  $E_{\min} = 1039$  GPa at  $\varphi \approx 45^\circ$  for LA6). Bulk moduli for TA6 and LA6 are also presented in **Table 7**. Bulk modulus is calculated as  $B = (c_{11} + c_{22} + c_{33} + 2c_{12} + 2c_{13} + 2c_{23})/9$ . Bulk moduli are 555 GPa for TA6 and 475 GPa for LA6 and they are higher than that for the other structures under consideration. Only CA7 fullerane has higher bulk modulus  $B = 694$  GPa.

The orientation dependences of shear modulus of carbon structures TA6 and LA6 for slip planes (100), (010), (001) are illustrated in **Figure 6**. The shear modulus for TA6 slightly changes in the slip planes (100), (010), (001). The shear modulus is constant in the slip plane (001) for LA6 and is equal to 442 GPa. In the case of slip planes (100) and (010), the maximum and

**Table 7.** Values of Young's modulus  $E$  and bulk modulus  $B$  for TA6 tubulane and LA6 DLP based on graphene.

Structure	$E_{[100]}$ [GPa]	$E_{[010]}$ [GPa]	$E_{[001]}$ [GPa]	$B$ [GPa]
TA6	1852	1852	1214	555
LA6	407	447	826	475

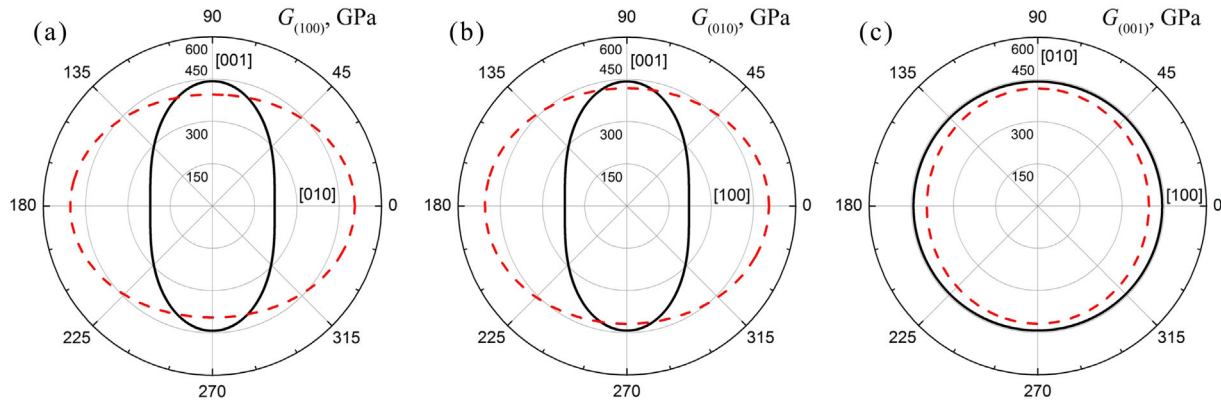


**Figure 6.** Orientational dependences of shear moduli in the (100) (a), (010) (b), (001) (c) planes for TA6 tubulane (black solid lines) and LA6 DLP based on graphene (red dashed lines).

**Table 8.** Extreme values of Poisson's ratio and values of Poisson's ratio in particular orientations for TA6 tubulane and LA6 DLP based on graphene.

Structure	$\nu_{\min}$	$\nu_{\max}$	$\nu_{[010],[100]}$	$\nu_{[001],[100]}$	$\nu_{[100],[010]}$	$\nu_{[001],[010]}$	$\nu_{[100],[001]}$	$\nu_{[010],[001]}$
TA6	-0.007	0.62	0.03	-0.007	0.03	-0.007	-0.005	-0.005
LA6	-0.14	0.66	0.57	0.14	0.63	0.06	0.29	0.11

minimum values of the shear modulus for the carbon structure LA6 differ by a factor of 1.53.

Analysis of the variability of Poisson's ratio for TA6 and LA6 structures shows that both structures are partial auxetics (see **Table 8** and **Figure 7**). The carbon structure of LA6 has a lower negative value of Poisson's ratio ( $\nu_{\min} = -0.14$ ) as compared to the tubulane TA6 ( $\nu_{\min} = -0.007$ ). It should be noted that the lower values of Poisson's ratio have structures CA7, TB and

fullerite is based on the  $C_{60}$  fullerene and the fullerene-like molecule  $C_{48}$ . Table 8 also shows Poisson's ratio for particular orientations. In these particular orientations, the negative Poisson's ratio is detected only in the tubulane TA6. Negative Poisson's ratio for LA6 is found when stretching in the direction  $\mathbf{n} = (0, -\sqrt{2}/2, \sqrt{2}/2)^T$  (i.e., at  $\varphi = 0$  and  $\theta = \pi/4$ ). The surface of auxeticity ( $\nu = 0$ ) for tubulane TA6 is presented. The zone of auxeticity ( $\nu < 0$ ) is located inside the closed surfaces.

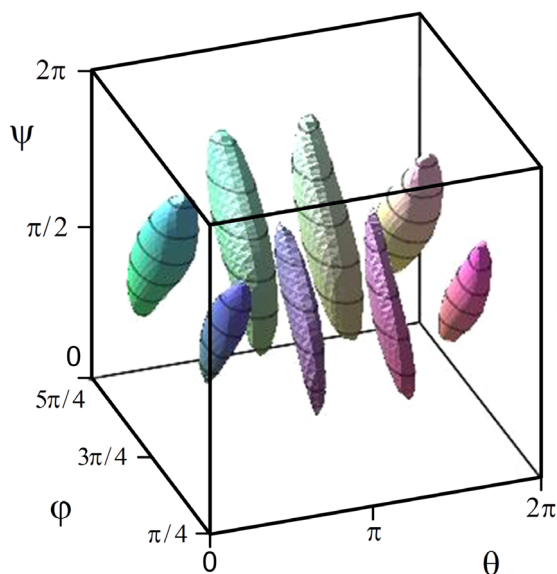


**Figure 7.** Auxeticity surface ( $\nu = 0$ ) for LA6 tubulane.

#### 4. Conclusion

The compliance and stiffness moduli for fullerites based on  $C_{60}$  and  $C_{48}$  fullerenes and for diamond-like phases based on fullerene-like molecules (CA2, CA3, and CA7), nanotubes (TA6, TB), and graphene (LA6) are obtained by MD simulation. All the structures are shown to be stable and can be elastically deformed until at least 1% strain. The results presented here show a qualitative agreement with the stiffness moduli of fullerite  $C_{60}$ , which have been found experimentally in ref. [44,45]. However, the calculated values are several times larger than the experimental. This difference can be explained by the fact that the experimentally obtained single crystals of fullerite can contain various defects, whereas calculations are performed for an ideal crystal at zero temperature.

From the stiffness and compliance coefficients the engineering elastic characteristics such as Young's modulus, Poisson's ratio and shear modulus are calculated by analytical methods. All the studied structures are partial auxetic, that is, they have negative Poisson's ratio for particular directions of uniaxial

strain. Minimal negative Poisson's ratio has TB tubulane ( $-0.80$ ). Young's modulus of TA7 tubulane is highest among the carbon nanostructures under consideration.

The study of the physical properties of this material is of great interest, since fullerite, and diamond-like phases can be used to create new composite materials, protective coatings, they can find applications in power engineering, biochemistry, and medicine.

## Acknowledgements

Calculation of the elastic coefficients for fullerite was done by R.L.Kh. and supported by the Russian Science Foundation, grant no. 14-13-00982. The calculation of the elastic constants for fullerenes was done by B.J.A. and supported by the Grant of the President of the Russian Federation for state support of young Russian scientists - doctors of sciences MD-1651.2018.2. The work of S.V.D. (discussion of the results) was supported by the Tomsk State University Competitiveness Improvement Programme. Calculation of the engineering elastic constants done by D.S.L. and V.A.G. was supported by the Russian Foundation for Basic Research, grant no. 16-01-00325 and the Federal Agency for Scientific Organizations (Project AAAA-A17-117021310373-3).

## Keywords

auxetics, carbon diamond-like phases, elastic properties, fullerites, molecular dynamics

Received: February 5, 2018

Revised: October 8, 2018

Published online: December 7, 2018

- [1] J. Q. Wang, C. X. Zhao, C. Y. Niu, Q. Sun, Y. Jia, *J. Phys.: Condens Matter* **2016**, *28*, 475402.
- [2] Z. Z. Li, C. S. Lian, J. Xu, L. F. Xu, J. T. Wang, C. Chen, *Phys. Rev. B* **2015**, *91*, 214106.
- [3] E. A. Belenkov, V. A. Greshnyakov, *Phys. Solid State* **2016**, *58*, 2145.
- [4] E. A. Belenkov, V. A. Greshnyakov, *Phys. Solid State* **2015**, *57*, 2331.
- [5] E. A. Belenkov, M. M. Brzhezinskaya, V. A. Greshnyakov, *Diamond Relat. Mater.* **2014**, *50*, 9.
- [6] E. A. Belenkov, V. A. Greshnyakov, *Phys. Solid State* **2013**, *55*, 1754.
- [7] D. S. Lisovenko, Y. A. Baimova, L. K. Rysaeva, V. A. Gorodtsov, S. V. Dmitriev, *Phys. Solid State* **2017**, *59*, 820.
- [8] D. S. Lisovenko, J. A. Baimova, L. K. Rysaeva, V. A. Gorodtsov, A. I. Rudskoy, S. V. Dmitriev, *Phys. Status Solidi B* **2016**, *253*, 1295.
- [9] J. A. Baimova, L. K. Rysaeva, A. I. Rudskoy, *Diamond Relat. Mater.* **2018**, *81*, 154.
- [10] M. M. Maslov, K. P. Katin, *Chem. Phys. Lett.* **2016**, *644*, 280.
- [11] K. P. Katin, V. S. Prudkovskiy, M. M. Maslov, *Physica E* **2016**, *81*, 1.
- [12] K. P. Katin, M. M. Maslov, *Adv. Condens. Matter Phys.* **2015**, *2015*, 1.
- [13] W. L. Mao, *Science* **2003**, *302*, 425.
- [14] K. Yamada, *Carbon* **2003**, *41*, 1309.
- [15] K. Yamada, Y. Tanabe, A. B. Sawaoka, *Philos. Mag. A* **2000**, *80*, 1811.
- [16] M. Miki-Yoshida, L. Rendón, M. José-Yacamán, *Carbon* **1993**, *31*, 843.
- [17] H. Tang, X. Yuan, P. Yu, Q. Hu, M. Wang, Y. Yao, L. Wu, Q. Zou, Y. Ke, Y. Zhao, L. Wang, X. Li, W. Yang, H. Gou, H. K. Mao, W. L. Mao, *Carbon* **2018**, *129*, 159.
- [18] N. V. Novikov, *J. Mater. Proc. Tech.* **2005**, *161*, 169.
- [19] R. A. Andrievski, *Int. J. Refract. Met. Hard Mater.* **2001**, *19*, 447.
- [20] Q. Zhu, A. R. Oganov, M. A. Salvadó, P. Pertierra, A. O. Lyakhov, *Phys. Rev. B* **2011**, *83*, 193410.
- [21] J. A. Baimova, L. K. Rysaeva, B. Liu, S. V. Dmitriev, K. Zhou, *Phys. Status Solidi B* **2015**, *252*, 1502.
- [22] J. A. Baimova, B. Liu, S. V. Dmitriev, K. Zhou, *J. Phys. D: Appl. Phys.* **2015**, *48*, 095302.
- [23] Y. A. Baimova, R. T. Murzaev, S. V. Dmitriev, *Phys. Solid State* **2014**, *56*, 2010.
- [24] J. A. Baimova, E. A. Korznikova, S. V. Dmitriev, B. Liu, K. Zhou, *Rev. Adv. Mater. Sci.* **2014**, *39*, 69.
- [25] A. V. Savin, E. A. Korznikova, S. V. Dmitriev, *Phys. Rev. B* **2015**, *92*, 035412.
- [26] A. V. Savin, E. A. Korznikova, I. P. Lobzenko, J. A. Baimova, S. V. Dmitriev, *Phys. Solid State* **2016**, *58*, 1278.
- [27] A. V. Savin, E. A. Korznikova, S. V. Dmitriev, E. G. Soboleva, *Comput. Mater. Sci.* **2017**, *135*, 99.
- [28] Y. A. Kvashnina, A. G. Kvashnin, L. A. Chernozatonskii, P. B. Sorokin, *Carbon* **2017**, *115*, 546.
- [29] A. Savin, R. Sakovich, M. Mazo, *Phys. Rev. B* **2018**, *97*.
- [30] A. Savin, M. Mazo, *Phys. Solid State* **2018**, *60*, 826.
- [31] A. Savin, S. Dmitriev, E. Korznikova, A. Kistanov, *Mater. Phys. Mech.* **2018**, *35*, 155.
- [32] A. Savin, M. Mazo, *Phys. Solid State* **2017**, *59*, 1260.
- [33] H. W. Kroto, J. R. Heath, S. C. O'Brien, R. F. Curl, R. E. Smalley, *Nature* **1985**, *318*, 162.
- [34] Z. G. Liu, H. Ohi, K. Masuyama, K. Tsuchiya, M. Umemoto, *J. Phys. Chem. Solids* **2000**, *61*, 1119.
- [35] L. Marques, Y. Skorokhod, R. Soares, *Carbon* **2015**, *82*, 599.
- [36] M. Popov, V. Mordkovich, S. Perfilov, A. Kirichenko, B. Kulnitskiy, I. Perezhogin, V. Blank, *Carbon* **2014**, *76*, 250.
- [37] M. Álvarez-Murga, J. L. Hodeau, *Carbon* **2015**, *82*, 381.
- [38] P. A. Heiney, J. E. Fischer, A. R. McGhie, W. J. Romanow, A. M. Denenstien, Smith, Cox, *Phys. Rev. Lett.* **1991**, *66*, 2911.
- [39] J. Tse, D. Klug, D. Wilkinson, Y. Handa, *Chem. Phys. Lett.* **1991**, *183*, 387.
- [40] M. N. Regueiro, P. Monceau, J. L. Hodeau, *Nature* **1992**, *355*, 237.
- [41] S. Hoen, N. G. Chopra, X. Xiang, R. Mostovoy, J. Hou, W. A. Vareka, A. Zettl, *Phys. Rev. B* **1992**, *46*, 12737.
- [42] X. D. Shi, A. R. Kortan, J. M. Williams, A. M. Kini, B. M. Savall, P. M. Chaikin, *Phys. Rev. Lett.* **1992**, *68*, 827.
- [43] N. P. Kobelev, R. K. Nikolaev, Y. M. Soifer, S. S. Khasanov, *Phys. Solid State* **1998**, *40*, 154.
- [44] N. P. Kobelev, *Phys. Solid State* **2002**, *44*, 195.
- [45] N. P. Kobelev, R. K. Nikolaev, N. S. Sidorov, Y. M. Soifer, *Phys. Solid State* **2002**, *44*, 429.
- [46] N. P. Kobelev, R. K. Nikolaev, N. S. Sidorov, Y. M. Soifer, *Phys. Solid State* **2001**, *43*, 2344.
- [47] G. V. Lier, C. V. Alsenoy, V. V. Doren, P. Geerlings, *Chem. Phys. Lett.* **2000**, *326*, 181.
- [48] F. Scarpa, S. Adhikari, C. Y. Wang, *J. Phys. D* **2009**, *42*, 142002.
- [49] V. R. Coluci, L. J. Hall, M. E. Kozlov, M. Zhang, S. O. Dantas, D. S. Galvão, R. H. Baughman, *Phys. Rev. B* **2008**, *78*, 115408.
- [50] F. Scarpa, S. Adhikari, A. S. Phani, *Int. J. Novel Mater.* **2010**, *1*, 39.
- [51] J. N. Grima, S. Winczewski, L. Mizzi, M. C. Grech, R. Cauchi, R. Gatt, D. A. K. W. Wojciechowski, J. Rybicki, *Adv. Mater.* **2015**, *27*, 1455.
- [52] J. A. Baimova, L. K. Rysaeva, S. V. Dmitriev, D. S. Lisovenko, V. A. Gorodtsov, D. A. Indeitsev, *Mater. Phys. Mech.* **2017**, *33*, 1.
- [53] R. V. Goldstein, V. A. Gorodtsov, D. S. Lisovenko, *Phys. Status Solidi B* **2016**, *253*, 1261.
- [54] F. Milstein, K. Huang, *Phys. Rev. B* **1979**, *19*, 2030.

- [55] R. H. Baughman, J. M. Shacklette, A. A. Zakhidov, S. Stafstrom, *Nature* **1998**, 392, 362.
- [56] T. C. T. Ting, D. M. Barnett, *J. Appl. Mech.* **2005**, 72, 929.
- [57] K. W. Wojciechowski, *Comput. Methods Sci. Techn.* **2005**, 11, 73.
- [58] A. N. Norris, *Proc. Roy. Soc. A* **2075**, 462, 3385.
- [59] T. Paszkiewicz, S. Wolski, *Phys. Status Solidi B* **2007**, 244, 966.
- [60] A. C. Branka, D. M. Heyes, K. W. Wojciechowski, *Phys. Status Solidi B* **2009**, 246, 2063.
- [61] R. V. Goldstein, V. A. Gorodtsov, D. S. Lisovenko, *Mech. Solids* **2010**, 45, 529.
- [62] Z. A. D. Lethbridge, R. I. Walton, A. S. H. Marmier, C. W. Smith, K. E. Evans, *Acta Mater.* **2010**, 58, 6444.
- [63] A. C. Branka, D. M. Heyes, K. W. Wojciechowski, *Phys. Status Solidi B* **2011**, 248, 96.
- [64] A. C. Branka, D. M. Heyes, S. Maćkowiak, S. Pieprzyk, K. W. Wojciechowski, *Phys. Status Solidi B* **2012**, 249, 1373.
- [65] R. V. Goldstein, V. A. Gorodtsov, D. S. Lisovenko, *Phys. Status Solidi B* **2013**, 250, 2038.
- [66] K. V. Tretiakov, K. W. Wojciechowski, *Phys. Status Solidi B* **2013**, 250, 2020.
- [67] R. V. Goldstein, V. A. Gorodtsov, D. S. Lisovenko, M. A. Volkov, *Phys. Mesomech.* **2014**, 17, 97.
- [68] V. V. Krasavin, A. V. Krasavin, *Phys. Status Solidi B* **2014**, 251, 2314.
- [69] P. M. Piglowski, K. W. Wojciechowski, K. V. Tretiakov, *Phys. Status Solidi RRL* **2016**, 10, 566.
- [70] K. V. Tretiakov, P. M. Piglowski, K. Hyzorek, K. W. Wojciechowski, *Smart Mater. Struct.* **2016**, 25, 054007.
- [71] A. I. Epishin, D. S. Lisovenko, *Tech. Phys.* **2016**, 61, 1516.
- [72] P. M. Piglowski, J. W. Narojczyk, K. W. Wojciechowski, K. V. Tretiakov, *Soft Matter* **2017**, 13, 7916.
- [73] V. A. Lubarda, M. A. Meyers, *Scripta Mater.* **1999**, 40, 975.
- [74] S. P. Tokmakova, *Phys. Status Solidi B* **2005**, 242, 721.
- [75] R. V. Goldstein, V. A. Gorodtsov, D. S. Lisovenko, *Dokl. Phys.* **2011**, 56, 602.
- [76] R. V. Goldstein, V. A. Gorodtsov, D. S. Lisovenko, *Dokl. Phys.* **2012**, 57, 174.
- [77] D. Gunton, G. Saunders, *J. Mater. Sci.* **1972**, 7, 1061.
- [78] N. Aouni, L. Wheeler, *Phys. Status Solidi B* **2008**, 245, 2454.
- [79] R. V. Goldstein, V. A. Gorodtsov, D. S. Lisovenko, M. A. Volkov, *Lett. Mater.* **2016**, 6, 93.
- [80] A. Ballato, *IEEE Trans. Ultrasonics Ferroelectrics Frequency Control* **1996**, 43, 56.
- [81] R. V. Goldstein, V. A. Gorodtsov, D. S. Lisovenko, M. A. Volkov, *Lett. Mater.* **2015**, 5, 409.
- [82] R. V. Goldstein, V. A. Gorodtsov, D. S. Lisovenko, *Phys. Mesomech.* **2015**, 18, 213.
- [83] M. Rovati, *Scripta Mater.* **2003**, 48, 235.
- [84] D. N. Karimov, D. S. Lisovenko, N. L. Sizova, B. P. Sobolev, *Crystallogr. Rep.* **2018**, 63, 96.
- [85] N. E. Novikova, D. S. Lisovenko, N. L. Sizova, *Crystallogr. Rep.* **2018**, 63, 438.
- [86] M. Rovati, *Scripta Mater.* **2004**, 51, 1087.
- [87] M. A. Volkov, *Lett. Mater.* **2014**, 4, 167.
- [88] Y. Li, *Phys. Status Solidi A* **1976**, 38, 171.
- [89] R. V. Goldstein, V. A. Gorodtsov, M. A. Komarova, D. S. Lisovenko, *Scripta Mater.* **2017**, 140, 55.
- [90] M. A. Komarova, V. A. Gorodtsov, D. S. Lisovenko, *IOP Conf. Ser. Mater. Sci. Eng.* **2018**, 347, 012019.
- [91] S. Plimpton, *J. Comp. Phys.* **1995**, 117, 1.
- [92] S. J. Stuart, A. B. Tutein, J. A. Harrison, *J. Chem. Phys.* **2000**, 112, 6472.
- [93] N. D. Orekhov, V. V. Stegailov, *J. Phys. Conf. Ser.* **2015**, 653, 012090.
- [94] G. M. Galiullina, N. D. Orekhov, V. V. Stegailov, *J. Phys. Conf. Ser.* **2016**, 774, 012033.
- [95] O. A. Shenderova, D. W. Brenner, A. Omeltchenko, X. Su, L. H. Yang, *Phys. Rev. B* **2000**, 61, 3877.
- [96] S. Winczewski, M. Y. Shaheen, J. Rybicki, *Carbon* **2018**, 126, 165.
- [97] Y. I. Sirotnin, M. P. Shaskolskaya, *Fundamentals of Crystal Physics*. Mir, Moscow **1982**.
- [98] R. V. Goldstein, V. A. Gorodtsov, D. S. Lisovenko, *Lett. Mater.* **2012**, 2, 21.
- [99] R. V. Goldstein, V. A. Gorodtsov, D. S. Lisovenko, *Lett. Mater.* **2011**, 1, 127.
- [100] R. V. Goldstein, V. A. Gorodtsov, D. S. Lisovenko, *Phys. Mesomech.* **2009**, 12, 38.